Available online at www.sciencedirect.com

ScienceDirect

Mendeleev Commun., 2021, **31**, 529–531

Mendeleev Communications

Nitrogen-enriched carbon powder prepared by ball-milling of graphene oxide with melamine: an efficient electrocatalyst for oxygen reduction reaction

Vladimir P. Vasiliev,* Roman A. Manzhos, Alexander G. Krivenko, Evgeny N. Kabachkov and Yury M. Shulga

Institute of Problems of Chemical Physics, Russian Academy of Sciences, 142432 Chernogolovka, Moscow Region, Russian Federation. E-mail: vpvasiliev@mail.ru

DOI: 10.1016/j.mencom.2021.07.031

A simple strategy for the production of an efficient platinum-free electrocatalyst for the oxygen reduction reaction was demonstrated. Nitrogen-enriched carbon powder was synthesized by a solid-phase method consisting of grinding graphene oxide and melamine in a planetary ball mill without any solvents and high-temperature processing. Based on XPS and IR spectroscopy data, it was assumed that the high electrocatalytic activity of the obtained material is due to the presence of nitrogen atoms and quinone groups on its surface.

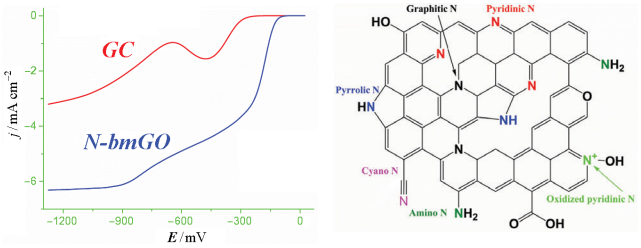

Keywords: graphene oxide, melamine, ball-milling, metal-free catalysts, oxygen reduction reaction.

Traditionally, catalysts in modern fuel cells with a polymer electrolyte membrane are platinum or platinum alloy nanoparticles on carbon black.[1–3] Concurrently, various carbon nanoforms, such as graphene-like structures, nanotubes and fullerenes, are intensively studied as supports for these catalysts. At the same time, conventional catalysts have obvious and fundamentally inevitable disadvantages, such as high costs and limited resources. Therefore, complex studies are needed to develop simple and effective methods for modifying carbon structures for their use as standalone platinum-free electrocatalysts for the oxygen reduction reaction (ORR) in fuel cells.[4] Carbon nanoforms doped with *p*-elements, such as nitrogen, are considered promising electrocatalysts for the ORR. The observed improved catalytic performance of the modified graphene-like structures is due to the electron-accepting ability of nitrogen atoms, which creates a net positive charge on adjacent carbon atoms in the graphene sheet.[5,6] It has been shown in several works[7,8] that the ORR on such structures proceeds along the four-electron pathway, which was previously[9,10] considered typical only for platinum and its alloys. However, the production of nitrogen-doped carbon nanoforms using well-developed methods is complicated by some problems, such as the toxicity of nitrogen sources, possible contamination of products with nitrogen precursors and the need for expensive special equipment.

In this study, we propose a simple synthesis strategy for producing nitrogen-doped carbon powder (N-bmGO) by grinding graphene oxide (GO) with melamine in a ball mill. The resulting material was characterized by scanning electron microscopy (SEM), X-ray photoelectron spectroscopy (XPS), infrared spectroscopy (IR) and Raman spectroscopy. Moreover, N-bmGO was tested as an ORR electrocatalyst and demonstrated a significant decrease in oxygen reduction overpotential and electron transfer numbers of 2.8–4.

It should be noted that there are very few publications on the mechanochemical approach[11] applied to carbon materials. In particular, ball-milling was previously used only for the exfoliation of graphite[12,13] and the production of carbon-based nanocomposites with transition metal oxides.[14,15]

GO was synthesized using the modified Hummers' method.[16,17] Its chemical composition corresponds to $C_8O_{4.6}H_{1.8}(H_2O)_{0.58}$. The nitrogen source was 99.9% pure melamine (BASF SE) (for details, see Online Supplementary Materials).

Figure 1 displays SEM images of an N-bmGO sample. As can be seen, GO sheets were ground during ball-milling, resulting in a powder-like matter with a grain size of 10–50 nm. Note that in Figure 1(*b*), only a small portion of the original GO sheet can be distinguished. According to the integrated intensities of the analytical lines in the survey XPS spectrum (Figure S1, see Online Supplementary Materials), the oxygen and nitrogen concentrations on the N-bmGO surface were 17.4 and 5.5 at%, respectively. It should be mentioned that milled GO was not only doped with nitrogen atoms but also partially reduced[18] as a result of mechanochemical synthesis. Indeed, the oxygen content in N-bmGO is *ca.* 6 at% lower than that in GO (Table S1).

Figure 2(*a*) presents the high-resolution C 1*s* spectrum of the N-bmGO sample and its deconvolution into five symmetric Gaussian–Lorentzian peaks. The peaks were assigned following the known data.[19–21] The dominant peak, C1, located at 284.5 eV, is typical for sp^2 carbon materials, and peak C2 corresponds to sp^3 hybridized carbon (Table 1). The second intense peak, C3, shifted by +2.1 eV from C1, can be attributed to carbon atoms linked by a single bond to oxygen or a double bond to nitrogen, that is, to hydroxy and epoxy groups or pyridinic and pyrrolic nitrogen. The next peak, C4, shifted by +3.5 eV, we assign to carbon atoms double-bonded to oxygen atoms (C=O) or single-bonded to

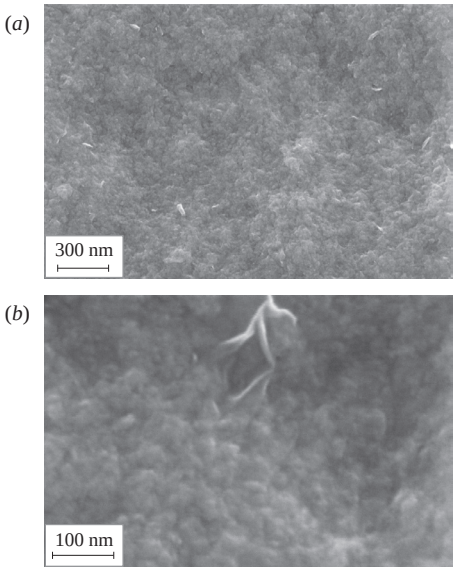

Figure 1 SEM images of the N-bmGO sample.

nitrogen. The last peak, C5, centered at 289.0 eV, can be attributed to the carbon atoms of the carboxyl group (O–C=O).

The high-resolution N 1*s* spectrum of the N-bmGO sample can be deconvoluted into three peaks [Figure 2(*b*), Table 1]. The assignment of these peaks following the literature data (see Online Supplementary Materials) allows us to conclude that pyrrolic nitrogen atoms make the main contribution to the N 1*s* spectrum. Note that catalytic activity in ORR is observed mainly for carbon materials containing active centers represented by pyridinic and graphitic nitrogen atoms.[22–25]

A distinctive feature of the IR spectra of carbon materials containing graphitic nitrogen is a high absorption intensity ranging from 1315 to 1350 cm^{-1}.[26] In our case, there is no noticeable absorption band in this region of the spectrum; therefore, we can assume the presence of a small amount of graphitic nitrogen in the sample, which is consistent with XPS data (Figure S2). The low absorption band at 3515 cm^{-1} indicates

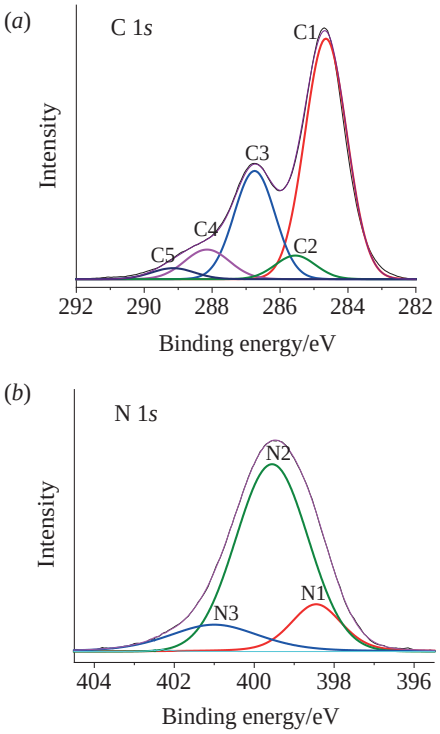

Figure 2 High-resolution (*a*) C 1*s* and (*b*) N 1*s* XPS spectra of the N-bmGO sample.

Table 1 Peak positions (E_b), full widths at half maximum (*FWHM*) and intensities (*Int*) of signals in the C 1*s* and N 1*s* XPS spectra of N-bmGO.

Peak	E_b/eV	*FWHM*/eV	*Int* (%)	Assignment
C1	284.5	1.5	52.6	C=C
C2	285.4	1.4	7.0	C–C
C3	286.6	1.5	28.2	C–O/C=N
C4	288.0	1.55	9.5	C=O/C–N
C5	289.0	1.6	2.7	O–C=O
N1	398.5	1.5	14.4	Pyridinic N
N2	399.6	2.1	71.0	Pyrrolic N
N3	401.0	2.6	14.6	Graphitic N

the presence of pyrrolic nitrogen (stretching vibrations of the N–H bond) in the N-bmGO sample. According to the published data,[27,28] the absorption band of the isolated pyrrole group is located at 3530.8 cm^{-1}. At last, in the spectrum of N-bmGO, one can see intense absorption bands in the region from 1650 to 800 cm^{-1}. For pure melamine, the absorption band at 1560 cm^{-1} can be attributed to the stretching vibrations of the triazine ring.[29,30] In our opinion, the vibrations of the pyrrole and pyridine rings are also in this range.

The Raman spectrum of N-bmGO shows peaks labeled D, D*, G, 2D, D + D' and 2D' (Figure S3). For N-bmGO, the positions of the D and G bands are shifted towards lower values compared to those for GO (Table 2), which indicates a decrease in the number of defects and the formation of graphene crystallites (graphitization)[31] in the N-bmGO sample. Based on the peak intensity ratio I_D/I_G = 1.67, the size of the sp^2 domain is *ca.* 11.5 nm.

Voltammograms measured in an oxygen-saturated solution of 0.1 M KOH for the bare glassy carbon (GC) electrode and the GC electrode loaded with N-bmGO are displayed in Figure 3(*a*). The number of electrons *n* participating in the ORR, determined at various potentials using the Koutecký–Levich equation,[31] is presented in Figure 3(*b*). Figure 3(*a*) shows that the oxygen reduction currents are higher for N-bmGO than for the bare GC electrode. On the voltammogram of N-bmGO [Figure 3(*a*), curve *2*], two waves of oxygen reduction can be distinguished. In the first wave, a linear increase in the cathodic current is observed in the potential range from –400 to –750 mV. The second wave demonstrates the limiting diffusion current of complete oxygen reduction to water at E < –900 mV. In this case, the corresponding value of the limiting diffusion current density obtained from the Levich equation[25,32] at n = 4 is j_d = –6.4 mA cm^{-2}. Note that in the potential range from –250 to –850 mV, the electron transfer number *n* increases linearly from 2.8 to 4 [see Figure 3(*b*)].

These data show that in the case of N-bmGO, even at low overpotentials, a reduction of O_2 to H_2O occurs alongside the oxygen reduction to hydrogen peroxide ($n \approx 2.8$ at $E \approx –200$ mV). The contribution of the first process to the overall oxygen reduction gradually increases with the potential scan in the negative direction until the complete reduction of oxygen to water at E < –850 mV ($n \approx 4$). Therefore, on the voltammogram

Table 2 Peak positions and band intensity ratio (I_D/I_G) in the Raman spectra of graphite, GO and N-bmGO.

Sample	Peak position/cm^{-1}		I_D/I_G
	D	G	
Graphite	1350	1582	0.04
GO	1374	1611	0.86
N-bmGO	1345	1393	1.67

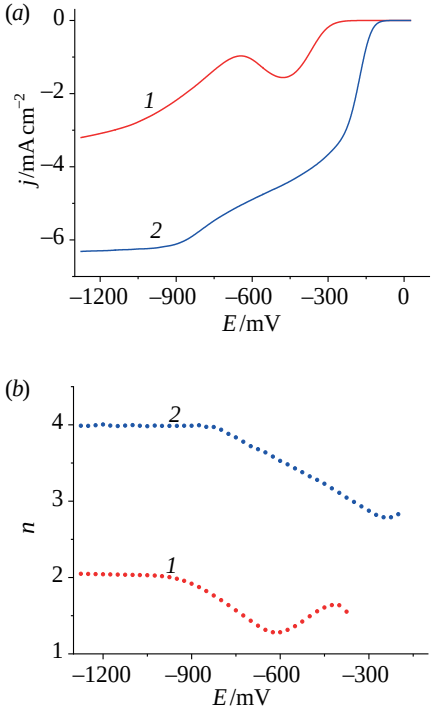

Figure 3 (*a*) Linear sweep voltammograms of an O_2-saturated 0.1 M KOH solution for (*1*) the bare GC electrode and (*2*) the GC electrode coated with N-bmGO at a potential scan rate of 10 mV s^{-1}, an electrode rotation rate of 2000 rpm and current density values corresponding to the geometric surface area of the electrodes. (*b*) Dependencies of the electron transfer number *n* on the potential *E* for (*1*) the bare GC electrode and (*2*) the GC electrode coated with N-bmGO.

for N-bmGO, the first wave corresponds to the O_2 reduction *via* two parallel pathways to form H_2O_2 and H_2O, and the second wave accounts for the oxygen reduction only to water. The half-wave potentials of the first wave of oxygen reduction for the GC electrode and N-bmGO are –360 and –180 mV, respectively. Thus, there is a significant difference in the ORR parameters for GC and N-bmGO. Namely, a decrease in the ORR overpotential (by 180 mV) and substantially higher values of *n* are observed for N-bmGO. The above facts imply a sufficiently high concentration of active centers on the N-bmGO surface for the adsorption of both oxygen and its reduction intermediates. These active centers can be represented by pyridinic nitrogen, graphitic nitrogen,[22,23,25] quinone groups,[32] surface defects and edge regions[33] of graphene-like structures.

In summary, we report a simple mechanochemical synthesis of an efficient platinum-free electrocatalyst for ORR. Nitrogen-enriched carbon powder obtained from inexpensive components, GO and melamine, exhibits a reasonably high catalytic activity in ORR, manifested in a decrease in the ORR overpotential and increased contribution of complete oxygen reduction to water to the overall process compared to GC. The approach proposed in this work can be effectively used to produce carbon nanomaterials with a certain degree of surface functionalization and doping with *p*-elements, which can be controlled by changing the time and grinding mode. Undoubtedly, the need for new carbon materials will stimulate further research in this area.

This study was performed within the framework of State Assignments nos. AAAA-A19-119032690060-9 and AAAA-A19-119061890019-5. R.A.M. and A.G.K. acknowledge the Russian Foundation for Basic Research (project no. 19-03-00310) for support in purchasing equipment and electronic components. Y.M.S. acknowledges the State program of basic research "For the long-term development and ensuring the competitiveness of society and the state" based on universities (project no. 0718-2020-0036). The work was carried out on the equipment of the Multi-User Analytical Center of the IPCP RAS and the Chernogolovka Scientific Center RAS.

Online Supplementary Materials

Supplementary data associated with this article can be found in the online version at doi: 10.1016/j.mencom.2021.07.031.

References

1 M. Shao, Q. Chang, J.-P. Dodelet and R. Chenitz, *Chem. Rev.*, 2016, **116**, 3594.
2 E. H. Majlan, D. Rohendi, W. R. W. Daud, T. Husaini and M. A. Haque, *Renewable Sustainable Energy Rev.*, 2018, **89**, 117.
3 Q. Shao, F. Li, Y. Chen and X. Huang, *Adv. Mater. Interfaces*, 2018, **5**, 1800486.
4 L. Dai, Y. Xue, L. Qu, H.-J. Choi and J.-B. Baek, *Chem. Rev.*, 2015, **115**, 4823.
5 L. Qu,Y. Liu, J.-B. Baek and L. Dai, *ACS Nano*, 2010, **4**, 1321.
6 K. Gong, F. Du, Z. Xia, M. Durstock and L. Dai, *Science*, 2009, **323**, 760.
7 N. Daems, X. Sheng, I. F. J. Vankelecom and P. P. Pescarmona, *J. Mater. Chem. A*, 2014, **2**, 4085.
8 K. Kakaei and G. Ghadimi, *Mater. Technol.*, 2021, **36**, 46.
9 K. Jukk, N. Kongi, K. Tammeveski, R. M. Arán-Ais, J. Solla-Gullón and J. M. Feliu, *Electrochim. Acta*, 2017, **251**, 155.
10 A. M. Gómez-Marín, J. M. Feliu and E. Ticianelli, *ACS Catal.*, 2019, **9**, 2238.
11 A. S. Rogachev, *Russ. Chem. Rev.*, 2019, **88**, 875.
12 V. León, A. M. Rodriguez, P. Prieto, M. Prato and E. Vázquez, *ACS Nano*, 2014, **8**, 563.
13 V. Priyanka, G. Savithiri, R. Subadevi, V. Suryanarayanan and M. Sivakumar, *New J. Chem.*, 2019, **43**, 16200.
14 J. Ahmad, F. A. Sofi, O. Mehraj and K. Majid, *Surf. Interfaces*, 2018, **13**, 186.
15 H. Kahimbi, S. B. Hong, M. Yang and B. G. Choi, *J. Electroanal. Chem.*, 2017, **786**, 14.
16 W. S. Hummers, Jr. and R. E. Offeman, *J. Am. Chem. Soc.*, 1958, **80**, 1339.
17 V. E. Muradyan, M. G. Ezernitskaya, V. I. Smirnova, N. M. Kabaeva, Yu. N. Novikov, Z. N. Parnes and M. E. Vol'pin, *J. Gen. Chem. USSR* (*Engl. Transl.*), 1991, **61**, 2514 (*Zh. Obshch. Khim.*, 1991, **61**, 2626).
18 O. Mondal, S. Mitra, M. Pal, A. Datta, S. Dhara and D. Chakravorty, *Mater. Chem. Phys.*, 2015, **161**, 123.
19 Y. Wang, F. Yu, M. Zhu, C. Ma, D. Zhao, C. Wang, A. Zhou, B. Dai, J. Ji and X. Guo, *J. Mater. Chem. A*, 2018, **6**, 2011.
20 F. Liu, F. Niu, T. Chen, J. Han, Z. Liu, W. Yang, Y. Xu and J. Liu, *Carbon*, 2018, **134**, 316.
21 G. Panomsuwan, N. Saito and T. Ishizaki, *ACS Appl. Mater. Interfaces*, 2016, **8**, 6962.
22 L. Lai, J. R. Potts, D. Zhan, L. Wang, C. K. Poh, C. Tang, H. Gong, Z. Shen, J. Lin and R. S. Ruoff, *Energy Environ. Sci.*, 2012, **5**, 7936.
23 D. Guo, R. Shibuya, C. Akiba, S. Saji, T. Kondo and J. Nakamura, *Science*, 2016, **351**, 361.
24 M. Figueras, I. J. Villar-Garcia, F. Viñes, C. Sousa, V. A. de la Peña O'Shea and F. Illas, *J. Phys. Chem. C*, 2019, **123**, 11319.
25 N. S. Komarova, D. V. Konev, A. S. Kotkin, V. K. Kochergin, R. A. Manzhos and A. G. Krivenko, *Mendeleev Commun.*, 2020, **30**, 472.
26 P. Lazar, R. Mach and M. Otyepka, *J. Phys. Chem. C*, 2019, **123**, 10695.
27 A. Mellouki, R. Georges, M. Herman, D. L. Snavely and S. Leytner, *Chem. Phys.*, 1997, **220**, 311.
28 I. Dauster, C. A. Rice, P. Zielke and M. A. Suhm, *Phys. Chem. Chem. Phys.*, 2008, **10**, 2827.
29 T. Hirayama and M. W. Urban, *Prog. Org. Coat.*, 1992, **20**, 81.
30 M. Sun, Y. Bu, J. Feng, C. Li, S. Han, X. Ji and J. Fan, *Microchem. J.*, 2020, **159**, 105573.
31 L. M. Malard, M. A. Pimenta, G. Dresselhaus and M. S. Dresselhaus, *Phys. Rep.*, 2009, **473**, 51.
32 V. P. Vasiliev, A. S. Kotkin, V. K. Kochergin, R. A. Manzhos and A. G. Krivenko, *J. Electroanal. Chem.*, 2019, **851**, 113440.
33 A. Shen, Y. Zou, Q. Wang, R. A. W. Dryfe, X. Huang, S. Dou, L. Dai and S. Wang, *Angew. Chem., Int. Ed.*, 2014, **53**, 10804.

Received: 15th March 2021; Com. 21/6491